DOE/ER/03992--476

DE82 014588

Multiplicity Distributions in Hadron-Hadron Collisions Based on the Universality Ansatz

by

Charles B. Chiu and Qu-bing Xie*

Center for Particle Theory, Department of Physics, University of Texas

Austin, Texas, 78712

*Permanent address: Department of Physics, Shandong University, Jinan, Shandong, People's Republic of China.

Abstract

Recent experiments on small-p_T hadron production in pp collisions have shed new light on the apparent violation of the universality ansatz that the multiplicity dispersion in hadron-hadron collisions is much larger than that in e^+e^- collisions. We present a model based on the universality ansatz, among other things. This model reproduces qualitatively the hadron multiplicity distributions in pp collisions over a wide range of energies. Within our framework, this essentially resolves the discrepancy stated above. In our approach the universality ansatz is also found to be applicable to the diffractive component events. This is supported by the inclusive x-distribution data having various specified number of prongs in the final states.

1. Introduction.

The notion that there should be a certain common feature in small-p_T hadron production among various two-body collision processes has been with us for sometime. In the usual confinement lore, the underlying dynamical mechanism for small-p_T hadronic production is presumably attributable to the separation of an energetic colored subsystem from an overall color-neutral system. Within this picture, the subsequent small-p_T hadron production due to color-separation should conceivably only depend on the quantum number and the energy of the escaping subsystem. And it should be insensitive to the details of the initial processes involved in preparing such a color-separation system. This then leads to the suggested idea of universality. An obvious place to test this universality idea is to compare the small-p_T production in hadron-hadron collisions where there are forward- and backward-jets to that in e^+e^- collisions in the energy region where two jets are dominating. However, we recall that there is a well-known apparent contradiction to this approach. In particular, at a given average multiplicity, the multiplicity dispersion in hadron-hadron collisions is substantially larger than that in e^+e^- collisions.[1]

Recent experiments have shed considerable light on this problem. For instance, in pp collisions at $\sqrt{s}$ = 62 GeV, Basile et al.[2,3] observed that after the removal of, say the right-moving leading positive charged particle with x between 0.4 and 0.8, the inclusive momentum distribution of the charged particles in the same hemisphere is similar to the corresponding inclusive distribution in e^+e^- collisions. Brick et al.[4] studied π^+p, K^+p and pp collisions at $\sqrt{s}$ = 16.7 GeV, where they selected those events with both the forward- and the backward-leading charged particles having $|x| > 0.3$. They

found that the average multiplicity and the multiplicity dispersion of the remaining hadronic system at a given effective energy $\sqrt{s_{eff}}$ is comparable to those in e^+e^- collisions at the corresponding energy $W = \sqrt{s_{eff}}$. Combining with the data of ref. 2, they found that the similarity in the average multiplicity persists essentially for all available energies ranging from $\sqrt{s_{eff}} = 1$ to 50 GeV. The corresponding similarity in the multiplicity dispersions has also been demonstrated in the energy region from $\sqrt{s_{eff}} = 1$ to 10 GeV. So it is apparently crucial to apply the universality assumption to the correct hadronic system.

Based on the empirical success of this universality idea, we come back to address once again the question: Why is the multiplicity dispersion in hadron-hadron collisions considerably larger than that in e^+e^- collisions? In general, with the universality assumption, one can use as input some information on e^+e^- collisions and the leading particle x-distributions in hadron-hadron collisions, through appropriate foldings of distributions to predict the corresponding information in hadron-hadron collisions. Basile et al.[3] have already taken a substantial step in this direction. They made Monte Carlo predictions on the fractional momentum distribution for hadrons in pp collisions based on fractional momentum distributions of hadrons produced in e^+e^- collisions together with the proton x-distribution in pp collisions. Their outcome is quite satisfactory. We follow a similar approach here. We find that the alluded discrepancy can be resolved at least qualitatively. In our approach the universality ansatz is also applied to diffractive events, which is supported by the fixed prong inclusive x-distribution data.

The outline of the remaining paper is as follows. In section 2, we describe a simple algorithm which spells out explicitly how the e^+e^- information

incorporated through the appropriate folding of distributions, leads to the prediction on the information in hadron-hadron collisions. Our discussion in this section is presented in the context of mulitplicity distributions, average multiplicity and multiplicity dispersion. In section 3, we discuss the parameterization of the spectator x-distribution and its quark model interpretation. In section 4, we compare our model predictions with hadron multiplicity data in pp collisions and with the leading particle x-distribution for final states having various specified prong-numbers. We end with some concluding remarks in section 5.

2. An Algorithm to Predict Multiplicities in Hadron-Hadron Collisions Based on e^+e^- Data

The work of refs. 2-4 naturally leads to a simple algorithm for correlating small-p_T hadronic processes in e^+e^- collisions and those in hadron-hadron collisions. Denote the magnitude of the longitudinal momentum fraction of the forward- and that of the backward-leading charged particles, in the cm system of the initial collision system at energy $\sqrt{s}$, by x_1 and $-x_2$, respectively. In the relativistic approximation, the effective energy of the remaining system is then given by

$$s_{eff} \approx s(1-x_1)(1-x_2) , \qquad \text{or} \quad \gamma^2 \equiv \frac{s_{eff}}{s} \approx (1-x_1)(1-x_2) . \qquad (1)$$

Since we will be dealing with pp collisions, we concentrate on the case where the projectile and the target particle are identical. Generalizations to other cases are straightforward. We assume that the longitudinal momentum distribution of the leading particle takes a scaling form, $P(x)$, and the

x-distribution of the right-moving and the left-moving leading particles are uncorrelated. The effective energy distribution, or equivalently the γ-distribution, of the remaining system can then be obtained as follows.

We introduce the generating function,

$$G = \int d\gamma^2 \, dx_1 dx_2 P(x_1)P(x_2)\delta(\gamma^2 - (1-x_1)(1-x_2)) = \int d\gamma dx_1 \frac{2\gamma P(x_1)P(x_2)}{1-x_1} ,$$

$$\text{where} \quad x_2 = 1 - \frac{\gamma^2}{1-x_1} . \tag{2}$$

Then the γ-distribution is given by the first order variation of G with respect to γ, i.e.

$$P_\gamma \equiv \frac{\delta G}{\delta \gamma} = 2\gamma \int_{x_o}^{x_m} dx_1 \frac{P(x_1)P(x_2)}{1-x_1} , \quad x_2 = 1 - \frac{\gamma^2}{1-x_1} , \tag{3}$$

where x_o and x_m are the appropriate cutoffs. For instance for the case of ref. 4, $x_o = 0.3$. When there is no additional experimental cutoff for large x, for fixed γ the upper limit is obtained through the relation:

$$x_m = \text{Max}(x_1) = \text{Max}\left(1 - \frac{\gamma^2}{1-x_2}\right) = 1 - \frac{\gamma^2}{1-x_o} . \tag{4}$$

Now we proceed to see how, with e^+e^- multiplicity distribution information as input, one obtains the corresponding quantity in hadron-hadron collisions. Denote the normalized multiplicity distribution for e^+e^- collisions at $W = \sqrt{s_{eff}} = \gamma\sqrt{s}$ by:

$$P_n(W) = P_n(\gamma\sqrt{s}) = \frac{\sigma_n}{\sum_n \sigma_n} . \tag{5}$$

Upon integrating over γ, the corresponding normalized multiplicity distribution for hadron-hadron collisions at cm energy $\sqrt{s}$ is given by

$$F_n(s) = \int_{\gamma_o}^{\gamma_m} d\gamma P_\gamma P_n(\gamma\sqrt{s}) \ , \tag{6}$$

where $\gamma_m = 1 - x_o$. The threshold energy for hadron final states in e^+e^- collisions is the two-pion mass. So we set $\gamma_o = 2m_\pi/\sqrt{s}$. Equation (6) is one of the main formulae to be used below, which relates the e^+e^- multiplicity distributions over a range of energies ($W = \gamma\sqrt{s}$) to hadron multiplicity distribution at the given energy $\sqrt{s}$.

There are also useful formulae which relate the average multiplicity $\bar{n}$ and multiplicity dispersion D'^2 in e^+e^- collisions to the corresponding quantities[5] in hadron-hadron collisions. More specifically, the latter at s are given by

$$\langle n(s)\rangle = \sum_n nF(s) = \int d\gamma P_\gamma \sum_n nP_n = \int d\gamma P_\gamma \bar{n}(\gamma\sqrt{s}) \ . \tag{8}$$

$$\begin{aligned} D^2(s) &\equiv \sum_n n^2 F_n(s) - \left(\sum_n nF_n(s)\right)^2 \\ &= \int d\gamma P_\gamma \sum_n n^2 P_n - \left(\int d\gamma P_\gamma \sum_n nP_n\right)^2 \\ &\equiv D_1^2(s) + D_2^2(s) \ , \end{aligned} \tag{9}$$

where

$$D_1^2(s) = \int d\gamma P_\gamma D'^2(\gamma\sqrt{s}) \ ,$$

and

$$D_2^2(s) = \int d\gamma P_\gamma \bar{n}^2(\gamma\sqrt{s}) - \left[\int d\gamma P_\gamma \bar{n}(\gamma\sqrt{s})\right]^2 \ .$$

Notice that the quantity D_1^2 is the dispersion squared obtained through averaging over the dispersion squared in e^+e^- collisions, while the quantity D_2^2 is the additional contribution to the dispersion squared due to the finite-width in the effective energy distribution, i.e. the extra dispersion due to the Doppler effects. We remark in passing that in Eq. (9) if P_γ is taken to be a distribution with a narrow width, the two terms in the expression for $D_2^2(s)$ will approximately cancel out each other. This is precisely the reason, when one experimentally measures D^2 for a given γ-bin, if there is universality one is essentially measuring directly the dispersion $D'^2(\gamma\sqrt{s})$ provided $\Delta\gamma$ is sufficiently small.

For the pp collision data at $p_{lab} = 147$ GeV, Brick et al.[4] choose the cutoff to be at $x = 0.3$. Based on their Table 1, using Eq. (9) above we obtain:

$$D_1^2 = 4.8,\ D_2^2 = 1.9 \text{ or } D^2 = 6.7.$$

On the other hand, with the inclusion of all events, in a separate paper,[6] the data from the same experiment by the same authors give $D^2 = 13.3$. Apparently a careful analysis of their data could provide the clue as to how the multiplicity dispersion of e^+e^- collision-type which is relatively small can finally be built up to that observed in pp collisions. So far, these authors have not yet addressed themselves to this question. Based on the algorithm stated above, below we present our calculation for hadron multiplicity distribution which attempts to account for the totality of the inelastic events.

3. The Spectator x-Distribution.

We divide the final states in hadron-hadron collisions into two categories:

the elastic and the inelastic events. We shall apply the universality ansatz to all inelastic events including those diffractive component events.[7] We shall justify this a posteriori.

Now we assume each inelastic final state event contains two parts: first the two spectator hadrons which carry some remnants of the initial hadrons and second, the remaining system. The small-p_T hadrons within the latter system are by the universality ansatz to behave in a similar manner as that in e^+e^- collisions. In ref. 4, it is found empirically that the universality phenomena are insensitive to the cutoff value x_o, so long as one identifies the spectators as the two forward- and backward-leading positive charged particles.[8] The experimental inclusive distributions for the leading proton for $x > 0.5$ at $p_{lab} = 102$ and 405 GeV are shown in Fig. 1. In this x-region, the leading proton contribution dominates. Below $x = 0.5$, at this stage the leading charged particle distributions are not available. We illustrate in the same figure, the x-dependence of the leading positive charged particles for events[9] with at least six prongs to serve as a crude guide. Notice in this $x < 0.5$ region there are two important features. As x decreases, first it gradually rises and second it turns over at around $x = 0.1$. This is the situation for final states with at least six prongs. Now for 2-prong and 4-prong events, we expect the leading particles to be relatively more energetic. Consequently, the resulting leading particle distribution for all events in the $x < 0.5$ region should give a milder rise for large x values (say near $x = 0.4$) and a slightly larger value for the onset of the turnover.

With the sharp rise in the x-distribution near $x = 1$ and a gradual rise in the distribution as x decreases below 0.5 in mind, we parameterize the spectator x-distribution by

$$P(x) = C\left(\frac{a}{1-x} + \frac{1}{\sqrt{x}}\right) . \qquad (10)$$

Here a is a parameter which is constrained by the proton inclusive distribution. The factor C is the appropriate normalization factor which assures $\int_{x_o}^{1} P(x)dx = 1$. On account of the observed turnover in the leading charged particle distribution for those ≥ 6 prong events there should be some effective lower limit for x_o. We have taken x_o to be a parameter in our fit. It turns out that our fit is not too sensitive to the precise value of x_o, so long as it is in the neighborhood of 0.1.

In Fig. 2, we illustrate a quark model interpretation for Eq. (10). For definiteness, we focus our attention on the top spectator. This spectator contains either one or two valence quarks from the top initial hadron, corresponding to respectively diagrams c,d,e,f and diagrams a,b. Near $x = 1$, those diagrams (a,b,d and f) which contain leading proton in the final state should dominate. In the Regge-Mueller language, this is given by the triple-Pomeron contribution. The x-dependence of the proton here is of the form of $(1-x)^{1-2\alpha_P}$. With the Pomeron intercept $\alpha_P = 1$, it leads to the first term in Eq. (10). For our typical solution presented below, $a = 0.04$. So this term is indeed important only near $x = 1$.

The second term of Eq. (10) is contributed by diagrams involving one initial valence quark in the spectator hadron. They correspond to diagrams c,d,e and f. In the small x-region, Regge-Mueller analysis leads to a behavior $x^{\alpha-1}$ for the spectator. With the nominal value of $\alpha = 1/2$, this leads to the form of the second term. This term has a long tail as x increases which is a welcome feature for describing the near constancy of the proton inclusive x-distribution in the region $x = 0.5$-0.9.

In Fig. 1, we also display our input P(x) distribution normalized to the data for our typical solution with a = 0.04. The agreement with the proton data for x > 0.5 is satisfactory.

4. Comparison with the Data.

a. Multiplicity distribution.

For the input charged hadron multiplicity distributions in e^+e^- annihilation, we make use of the information obtained by Berger et al.[1] at Petra energies. Their data at 9.4 GeV and at 30.7 GeV are shown in a KNO plot given in Fig. 3. The solid curve is a fit[10] to the corresponding data of $\bar{p}p$ annihilations, which describes the e^+e^- data reasonably well. We take this curve as the approximate representation of the multiplicity distributions in e^+e^- collisions for average charge multiplicity $\bar{n} \geq 2$. For $\bar{n}$ less than 2, we use a Poisson distribution for the corresponding multiplicity distribution. The KNO curve is given by:

$$P_n = \frac{\sigma_n}{\sigma} = \frac{1}{\bar{n}} \psi(z) \ , \tag{11}$$

with

$$z = \frac{n}{\bar{n}} \quad \text{and} \quad \psi(z) = \exp[-3.31 + 8.76z - 5.3z^2 + 0.6z^3] \ .$$

For average multiplicity of charged hadrons in e^+e^- collisions, we use the form

$$\bar{n} = (3.46 + 7W)^{\frac{1}{2}} - 1.86 \ , \tag{12}$$

which gives an overall fit to the e^+e^- data,[11] see Fig. 4. Based on Eqs. (3), (6), (11) and (12), we calculated the multiplicity distributions for pp collisions. There are two adjustable parameters. We present below our predictions for a typical solution with $a = 0.04$ and $x_o = 0.1$. Our predictions compared to multiplicity distributions in the ISR energy region[6] for $\sqrt{s}$ = 24, 31, 45, 51 and 63 GeV are shown in Fig. 5. The agreement is very satisfactory.

The comparison between theoretical prediction and the data[12,13] for $\langle n \rangle$ versus ln s and D versus $\langle n \rangle$ are shown in Figs. 6 and 7 respectively. Again the overall agreement over a wide range of energy is very encouraging. Within the present framework, we see how large dispersions of hadron-hadron collisions are built up from relatively small dispersions in e^+e^- collisions. The crucial point lies in the P(x) distribution. Apparently the combined effect of having a sharp peak near $x = 1$ and a milder peak in the small x-region gives rise to a wide distribution in P_γ and, in turn, a large D_2^2 term in Eq. (9). Fig. 7 shows quantitatively the amount of enhancement in the dispersion which we obtain beyond that for the e^+e^- case.

The circular solid point in Fig. 7 corresponds to the pp data[6] at $p_{lab} = 147$ GeV. The corresponding multiplicity distribution in a KNO plot compared with the various hadron-proton collision data[6,14] is illustrated in Fig. 8. In the same figure the input KNO curve for e^+e^- of Eq. (11) is also included for comparison. Besides the fact that the error bars of the pp data given in Fig. 8 are substantially smaller than those at ISR given in Fig. 5, the quality of the agreement between the theoretical curve and the pp data in this energy region is not as good as that at higher energies. Nevertheless, our curve shows a definite broadening over the corresponding e^+e^- KNO

curve, and our curve is also in qualitative agreement with the pp data, and also other hadron-proton data.

The typical solution we presented here is originally obtained to fit the highest ISR energy multiplicity distribution data at $\sqrt{s} = 63$ GeV. So at other energies, the predictions are essentially parameter-free. At this stage, in view of the simplicity of the present model, no attempt has been made to systematically vary the parameters: x_o and a, to achieve an overall best fit to all data considered.

b. Leading particle x-distribution at various fixed number of prongs.

To facilitate our comparison with the experimental leading-particle x-distributions for various fixed number of prongs, we return to Eq. (2). Taking the first order variation of G with respect to x, we get

$$f(x) = \frac{\delta G}{\delta x} = \int_{\gamma_o}^{\gamma'_m} 2\gamma \frac{P(x)P(x_2)}{1-x} d\gamma \ , \tag{13}$$

where

$$x_2 = 1 - \frac{\gamma^2}{1-x} \ , \quad \gamma'_m = \text{Max}\ \sqrt{(1-x)(1-x_2)} = \sqrt{(1-x)(1-x_o)} \ .$$

Here, as a consistency check, we can also calculate the normalized multiplicity distribution in pp collisions by integrating over x. This gives

$$F_n(s) = \int_{x_o}^{x'_m} dx \int_{\gamma_o}^{\gamma'_m} d\gamma \frac{2\gamma P(x)P(x_2)}{1-x} P_n(\gamma\sqrt{s}) \ , \tag{14}$$

with

$$x'_m = 1 - \gamma_o^2/(1-x_o) \ .$$

In our numerical calculations, we did calculate $F_n(s)$ using both methods of Eqs. (6) and (14). We have verified that within the accuracy of our calculation the two methods agree with each other.

The comparison between theoretical predictions at p_{lab} = 102, 205 and 405 GeV and the data[7] are shown in Fig. 9. At each energy the relative normalization within each diagram, i.e. 9a, 9b, 9c and 9d are predicted by the theory. However, to facilitate the comparison on the x-dependence between theoretical predictions and the data, we have multiplied the theoretical curves in Figs. 9c and 9d by a factor 0.6.

The close agreement between the x-dependence of the theory and the data displayed in Fig. 9 is quite remarkable. Apparently our original assumption that the universality ansatz is applicable to the diffractive component appears to be not unreasonable.

Our prediction for various fixed-prong events up to an overall normalization at $\sqrt{s}$ = 63 GeV is shown in Figs. 9b and 9d. Notice in particular that we predict a definite peak near x = 1 for the 6- and 8-prong events. It is interesting to verify these predictions experimentally.

5. Concluding Remarks.

We have constructed a simple model to illustrate that the dominant multiplicity featuers observed in pp inelastic collisions can be accounted for by the universality ansatz. In our approach it is not necessary for us to introduce an additional component to describe the so-called diffractive events. What we have found is that so long as we have included the sharp peak near x = 1 in the P(x) distribution, the diffractive component is automatically included in our model. In the calculation of Basile et al.,[3] they carefully

excluded this peak. From our point of view this is not necessary. The good agreement between the theoretical curves and the data on the x-dependence of the leading particles for the various fixed prong events lends support to our proposal.

Furthermore, in order to reproduce the large dispersion in pp collisions, it is also important for us to consider the P(x) distribution with a peak in the small x region. Such a peak would be absent if one follows the proposal of ref. 3, where the corresponding spectator x-distribution is identified as the proton inclusive distribution over the entire x-region.

Admittedly there are some oversimplified assumptions introduced in our calculation, such as the specific parameterization and the cutoff introduced for the P(x) distribution, and the KNO scaling form for the e^+e^- multiplicity distributions. Fortunately these are basically experimental quantities. They can be improved on by future experiments. From our point of view, it is important to further carry out experimental analysis on the leading charge particle distribution especially in the small x-region. One should also examine: What are the additional effects, when one takes into account the leading neutral particles? Furthermore, it is useful to extend the present analysis to other hadron-hadron interactions. This is particularly so in view of the fact that other hadron-proton interactions as illustrated in Fig. 8 have the multiplicity distributions which are similar to those for pp interactions.

A few words of caution on the application of the universality ansatz are in order here. Recent experiments have taught us that one should be careful in defining the hadronic system in hadron-hadron collisions where the ansatz is to be applied. In particular there could be confusion due to Doppler effects. However, one can use the spectators as a guide to remove

this confusion. We stress here that in the application of the universality ansatz, we have implicitly restricted ourselves to small-p_T hadronic production events. Fortunately in hadron-hadron collisions, large-p_T events are rarities. We are not making many mistakes, even when we include some large-p_T events in the totality of inelastic events we are considering.

For the application of the universality ansatz in e^+e^- collisions we should also be discreet about the types of final states which are admissible. To make the correspondence, one should again restrict oneself to those small-p_T hadronic final states. This is important since we are interested only in the samll-p_T or the soft hadronic production processes where the confinement dynamics dominates. Once the p_T is sufficiently large, one enters into the perturbative QCD domain for hadron production where the universality is certainly not applicable.

In this context, the empirical success of the universality ansatz also reflects that in e^+e^- collisions at present energies, the small-p_T hadronic production mechanism still plays an important role. There are still substantial small-p_T hadronic events among all possible final states in e^+e^- collisions.

After completion of the present manuscript, it was called to our attention a paper by K. Fialkowski and A. Kotanski, Phys. Lett. 107B, 132 (1981), in which the multiplicity of dispersion of charged hadrons in pp collision is considered based on a two-chain dual model. They found that based on the universality ansatz, after correcting the energy spread effect and including the diffractive component events, they can explain the large dispersion in pp data. Although the present approach and that of theirs differ in detail, so

far as the applicability of the universality ansatz is concerned, the two approaches arrive at essentially the same conclusion.

Acknowledgement: We would like to thank Dr. R. Hulsizer and Dr. J. Goldberg for invaluable discussions related to their data. We would like to thank Professor George Sudarshan and Professor S. P. Chia for discussions and careful reading of the manuscript. One of us (QBX) would like to express his gratitude to Professor Sudarshan and colleagues in the Center for Particle Theory for the hospitality extended to him during his six-month visit at the Center. This work is supported in part by the U.S. Department of Energy.

References and Footnotes

1. Pluto collaboration, Ch. Berger et al., Phys. Lett. 95B, 313 (1980).
2. M. Basile et al., Phys. Lett. 92B, 367 (1980).
3. M. Basile et al., Nuovo Cimento 58A, 193 (1980).
4. D. Brick et al., Phys. Lett. 103B, 241 (1981).
5. When comparing the average charged multiplicity in pp collisions $\langle n \rangle$, with that in e^+e^- collisions $\bar{n}$, one should take into account the initial two units of positive charges in pp collisions, and compare the quantity $\langle n \rangle - 2$ with $\bar{n}$.
6. Multiplicity distributions of charged hadrons in pp collisions:
   a. At p_{lab} = 147 GeV (also include K^+p and π^+p data), D. Brick et al, 1981, unpublished, see Table 6 and Fig. 9 there in.
   b. At ISR energies: W. Thome et al., Nucl. Phys. B129, 365 (1977), see Fig. 15.
7. The diffractive component events and the inclusive x-distribution of protons in pp collisions:
   a. Data at 102 and 405 GeV, J. W. Chapman et al., Phys. Rev. Letters 32, 257 (1974).
   b. Data at 205 GeV, S. J. Barish et al., Phys. Rev. Letters 31, 1080 (1973).
8. Also private communication from R. I. Hulsizer and J. Goldberg, two of the authors of ref. 4.
9. The x-distribution for fastest charged particles in events with six prongs or greater in pp collisions at p_{lab} = 147 GeV is given by S. H. Oh, "Quark-Parton and the Low Temperature Momentum Hadron-Hadron

Interaction," MIT Ph.D. Thesis, 1981 (unpublished). The forward hemisphere data are from his Fig. 45c and the backward hemisphere data from Fig. 46a.

10. J. Salava and V. Simak, Nucl. Phys. 69B, 15 (1974).

11. See Fig. 1b of ref. 4.

12. Average multiplicity of charged hadrons in pp collisions:

    a. E. Albini et al., Nuovo Cimento 32A, 101 (1976).

    b. W. Thome et al. of ref. 6b, see Table 3 therein.

13. Multiplicity dispersion versus average multiplicity:

    (i) pp data:

        a. W. Thome et al. of ref. 6b, see Table 3 and Fig. 20 therein.

        b. See also D. Brick et al. of ref. 6a.

    (ii) e^+e^- data:

        c. See Table 1 of Pluto collaboration of ref. 1.

14. P. Slattery, Phys. Rev. Letters 29, 1624 (1972).

Figure Captions

Fig. 1. Our input x-distribution curve for the spectators compared to the leading charge particle data in pp collisions. Data for $x > 0.5$ are taken from ref. 7a. The histogram is at $p_{lab} = 102$ GeV and the black dots at 405 GeV. Dashed bars are from ref. 9. They are the x-distributions for leading favored charged particles with arbitrary normalization, taken from events which have six or more prongs in the final states. The upper and lower limits indicate experimental variations between mean values of the forward hemisphere data and those of the backward hemisphere data.

Fig. 2. Quark model diagrams illustrating the various possibilities of the initial valence quark contents in the two spectators.

Fig. 3. Multiplicity distributions of charged hadrons in e^+e^- collisions shown in a KNO plot. Data points are taken from ref. 1. Crosses are at 9.4 GeV and dots at 30.7 GeV. The solid curve is for $\bar{p}p$ annihilation. It is from ref. 10.

Fig. 4. Average multiplicity of charged hadrons in e^+e^- collisions versus collision energy W. The curve is our empirical fit of Eq. (12) to the data. For the data points see ref. 4, Fig. 1b therein.

Fig. 5. The predicted normalized multiplicity distributions of charged hadrons in pp collisions compared to the data of ref. 6b at ISR energies.

Fig. 6. Average multiplicity of charged hadrons in pp collisions versus $\ln s$. Solid curve is our prediction. For data points see ref. 12.

Fig. 7. Comparison between the dispersion of charged hadron multiplicities as a function of average multiplicity in pp collisions and that in e^+e^- collisions. For the pp case, the open circle data points are from ref. 13a and the circular solid point is from ref. 13b. For the e^+e^- case, $\langle n \rangle = \bar{n} + 2$ is used (see ref. 5). The triangular data points are from ref. 13c and the dashed line is drawn to guide the eye.

Fig. 8. Comparison of multiplicity distribution of charged hadrons in a KNO plot, between various hadron-proton collisions and e^+e^- collisions. Data points for various hadron-proton collisions are taken from ref. 6a. Notce that our predicted curve for pp collisions (solid curve) is in between the e^+e^- curve (dashed curve of Eq. (11)) and the KNO curve (dashed-dot curve) of ref. 14 for pp collisions.

Fig. 9. Comparison between the predicted leading charged particle x-distribution for various specified number of prongs at several energies and the data. The data at $p_{lab} = 102$ and 405 GeV are from ref. 7a and at 205 GeV from ref. 7b. Notice that the predicted curves at $p_{lab} = 2100$ GeV (or $\sqrt{s} = 63$ GeV) show peaks near $x = 1$ for the 6- and 8-prong events. For comments on the normalizations of the curves shown, see text.

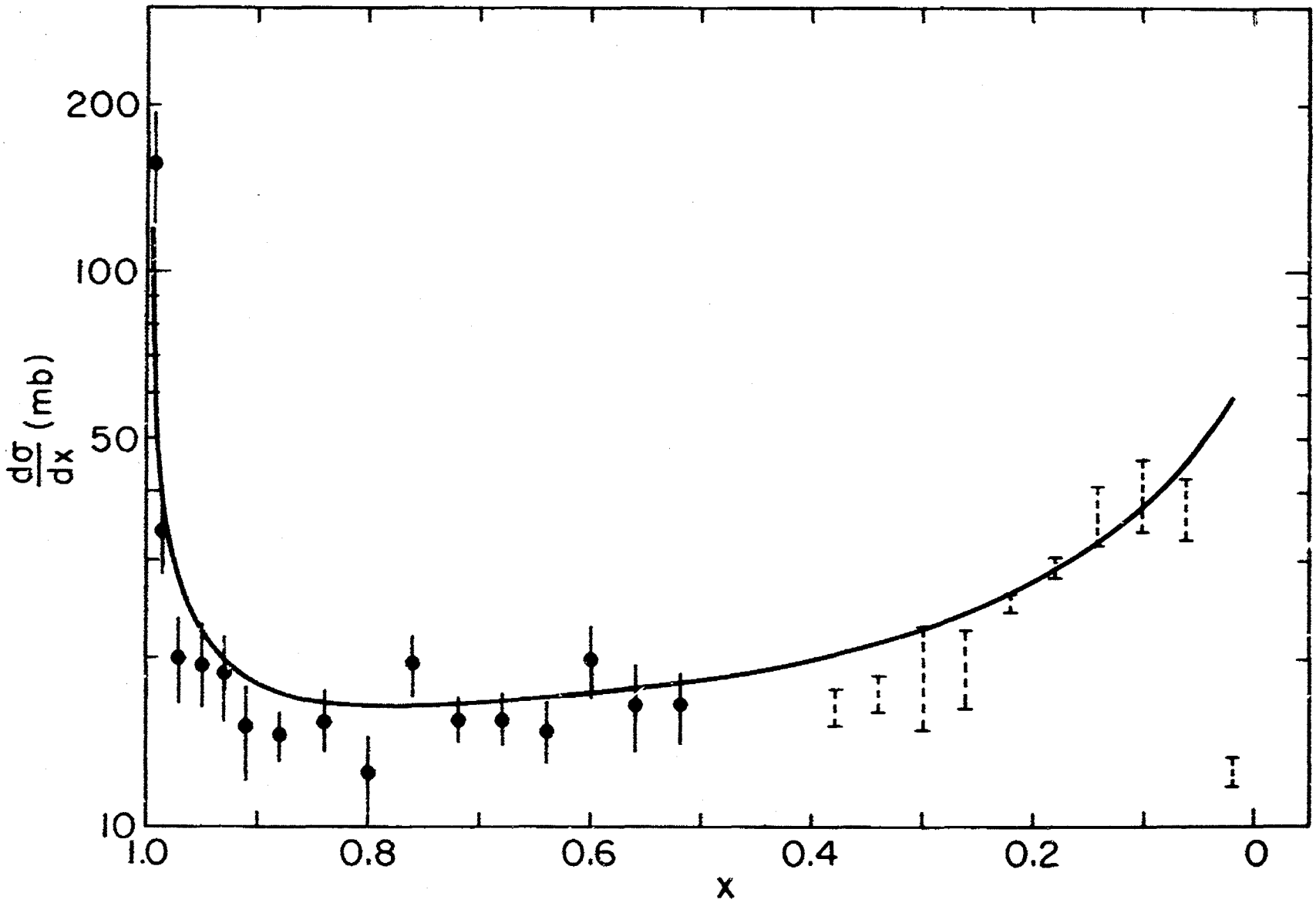

Fig. 1

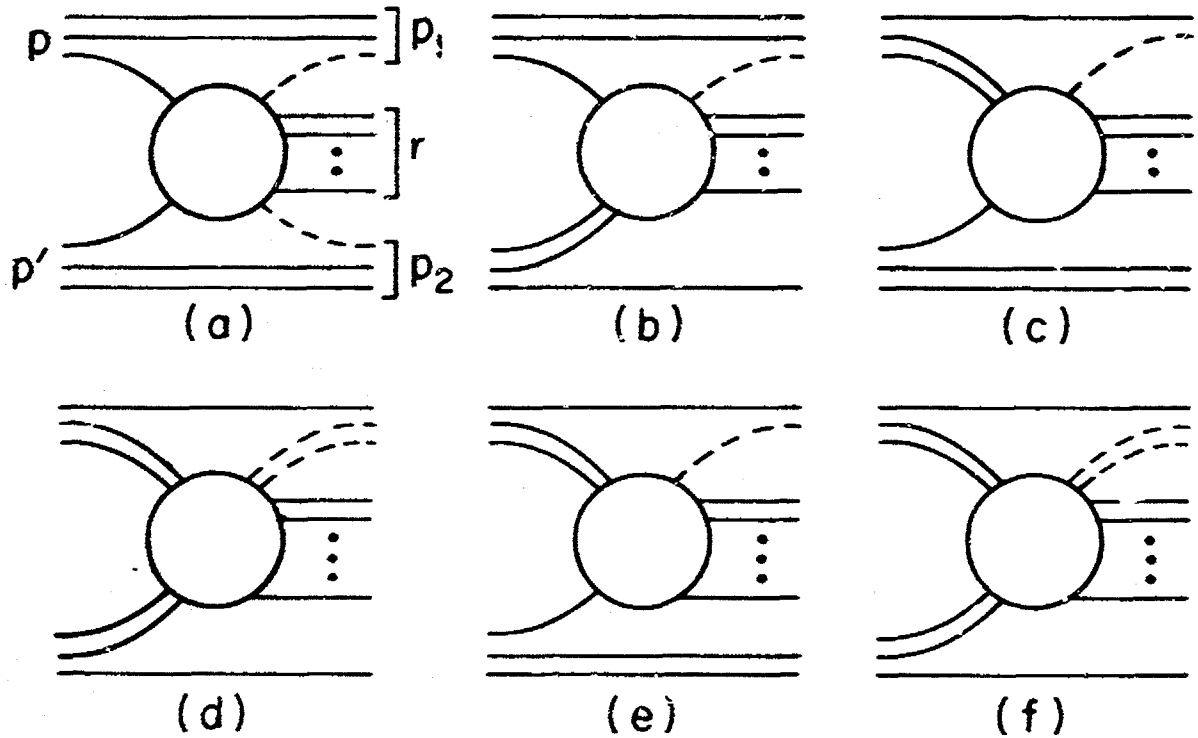

Fig. 2

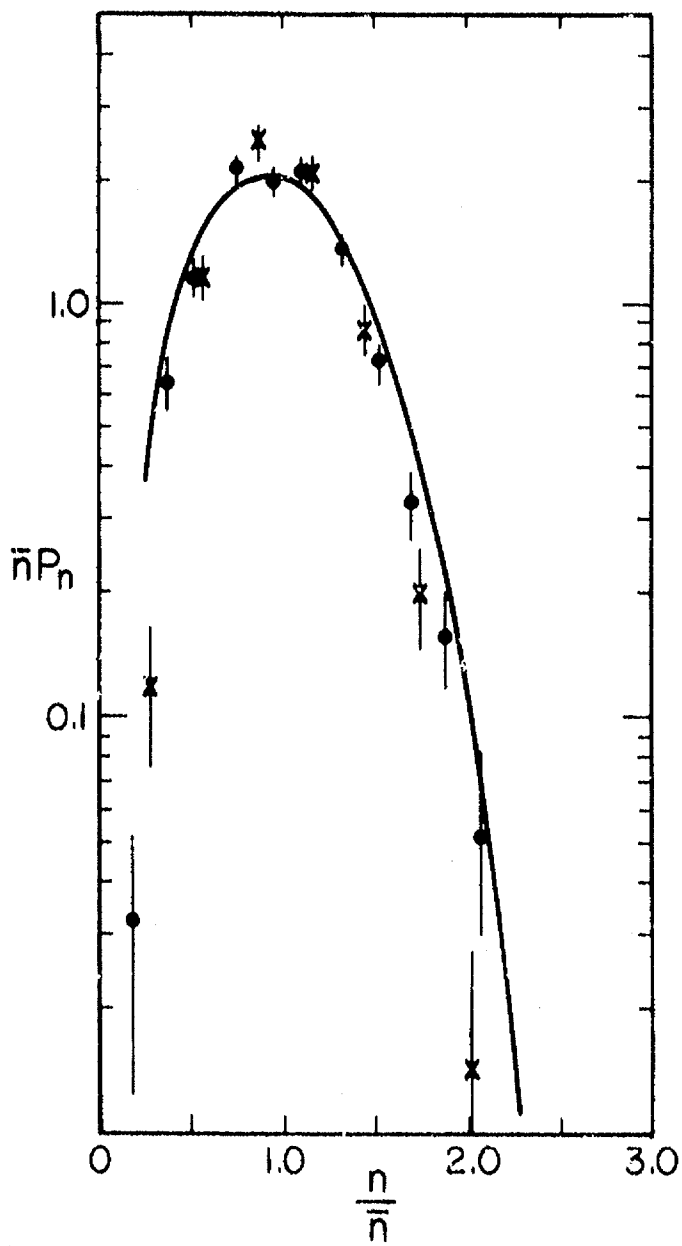

Fig. 3

Fig. 4

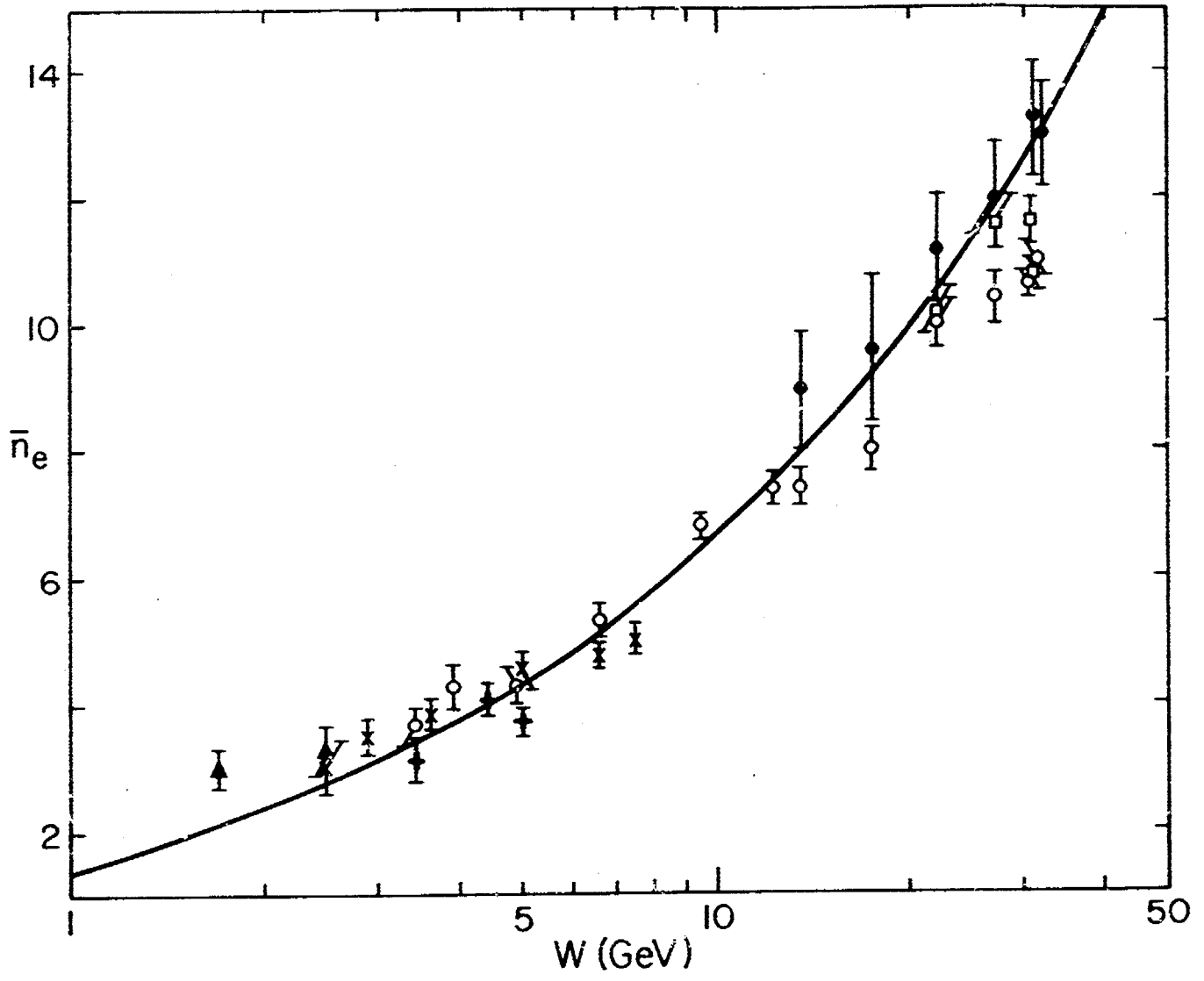

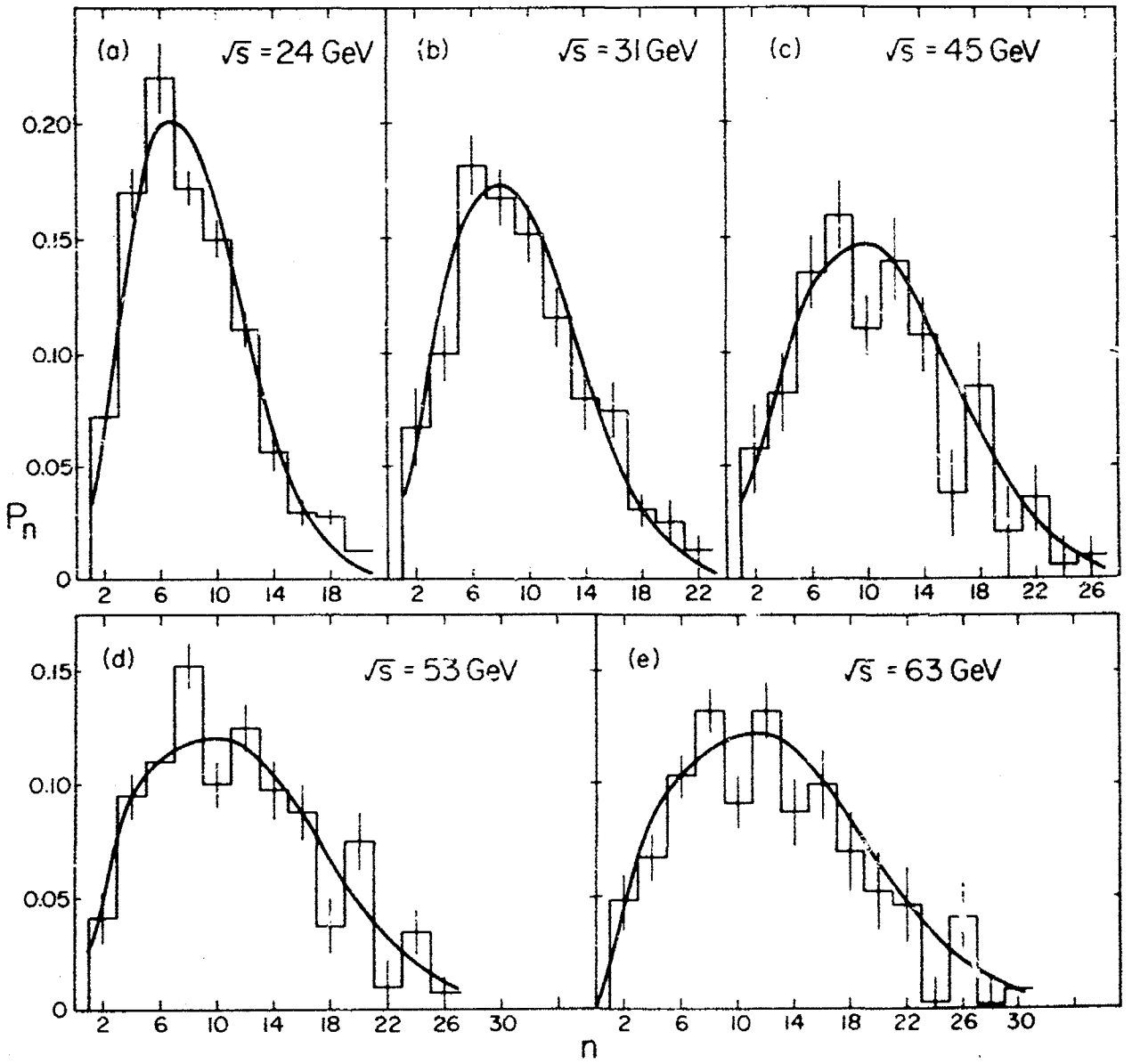
(a) √s = 24 GeV
(b) √s = 31 GeV
(c) √s = 45 GeV
(d) √s = 53 GeV
(e) √s = 63 GeV
Pn
n
0.20
0.15
0.10
0.05
0
2 6 10 14 18
2 6 10 14 18 22
2 6 10 14 18 22 26
0.15
0.10
0.05
0
2 6 10 14 18 22 26 30
2 6 10 14 18 22 26 30

Fig. 5

Fig. 6

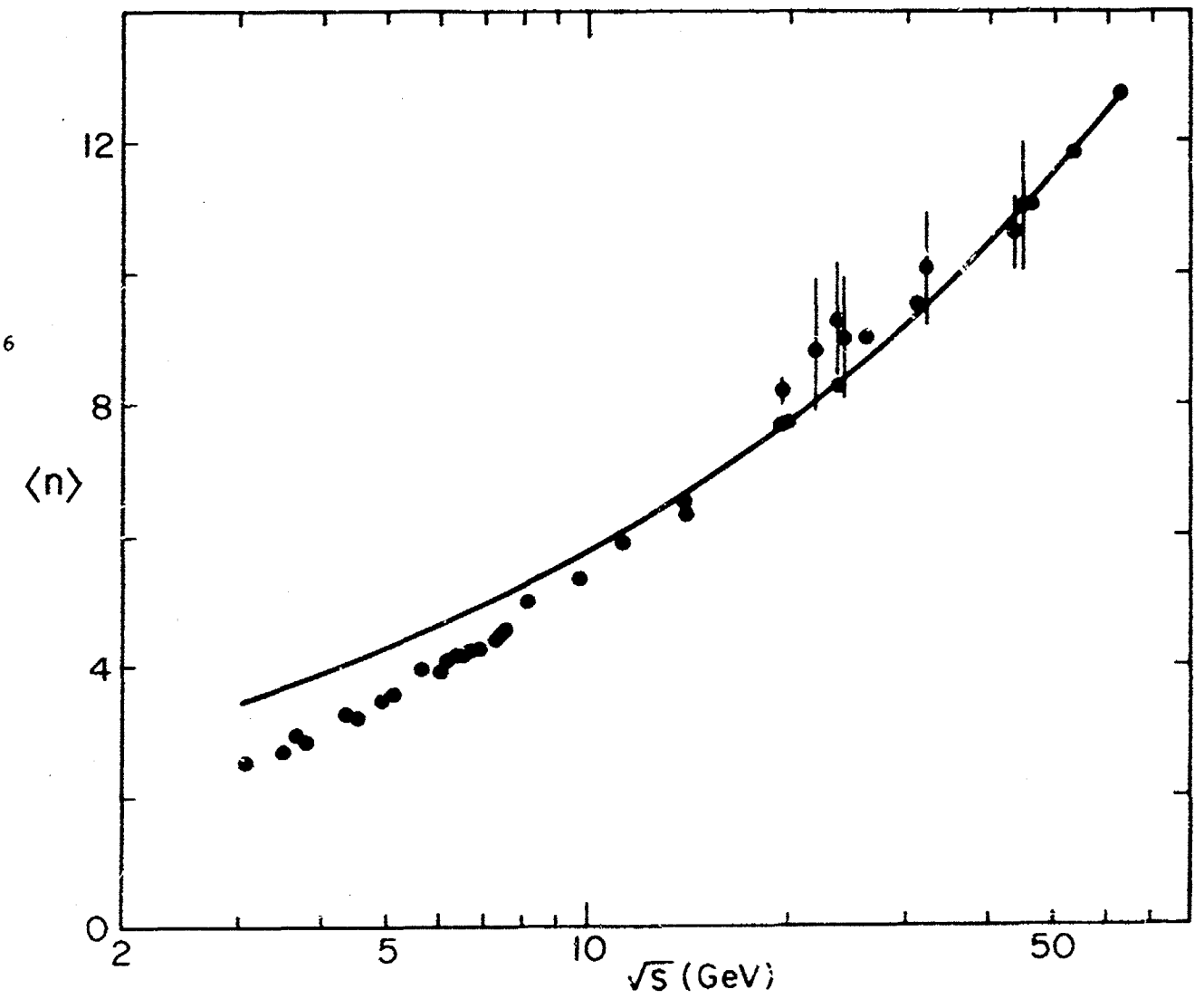

Fig. 7

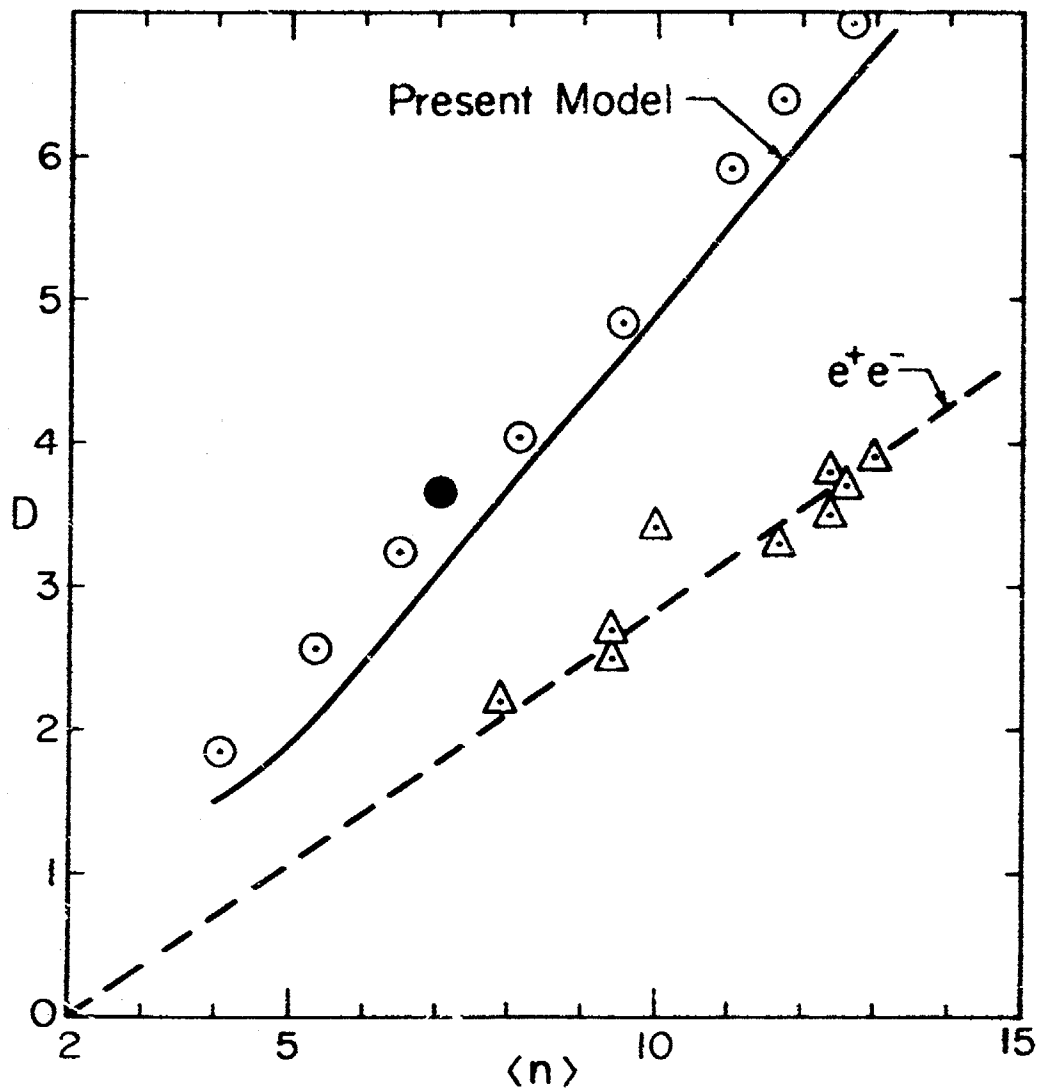

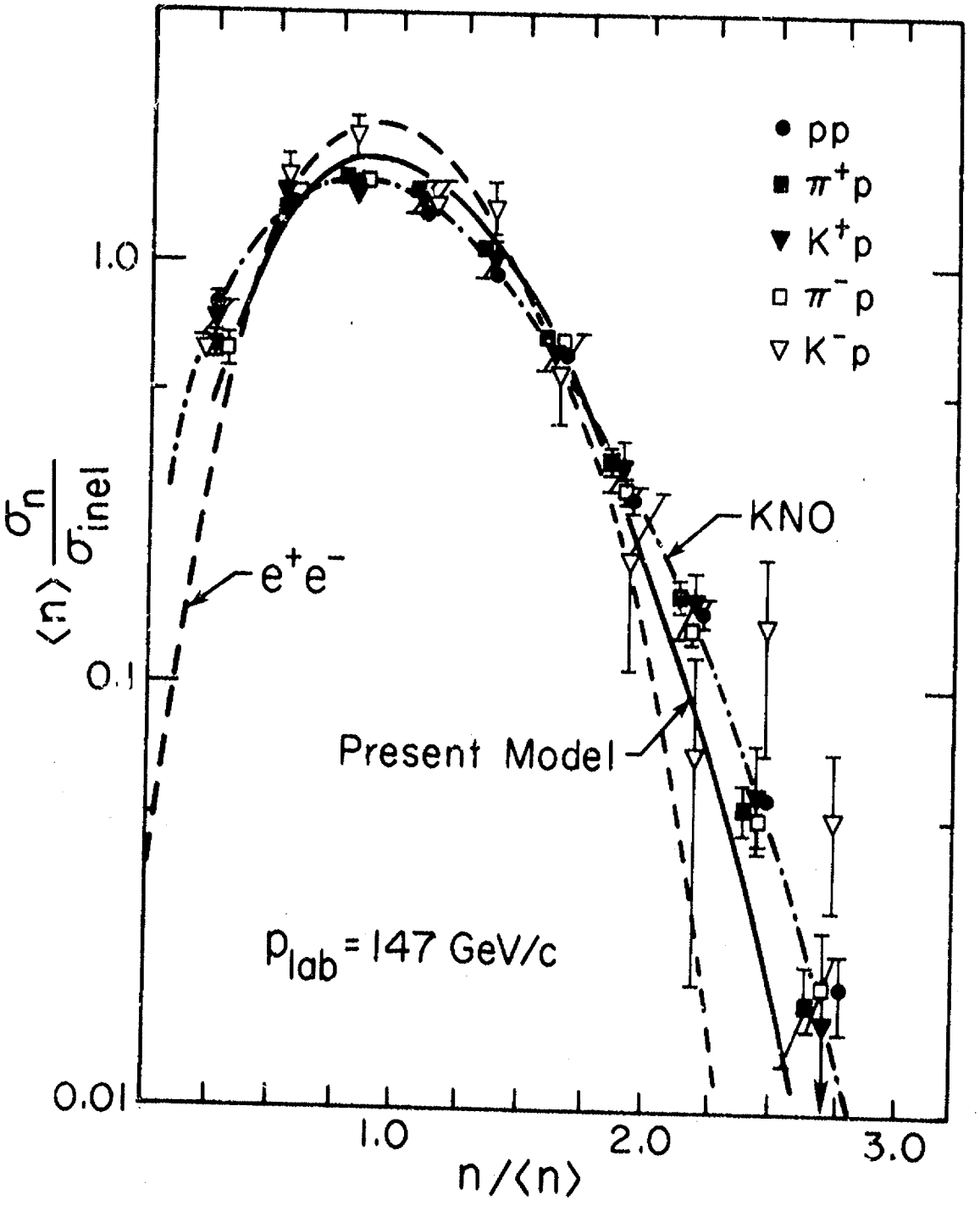
pp
π^+p
K^+p
π^-p
K^-p
KNO
e^+e^-
Present Model
$p_{lab} = 147$ GeV/c
$\frac{\sigma_n}{\langle n \rangle \sigma_{inel}}$
1.0
0.1
0.01
1.0
2.0
3.0
$n/\langle n \rangle$

Fig. 8

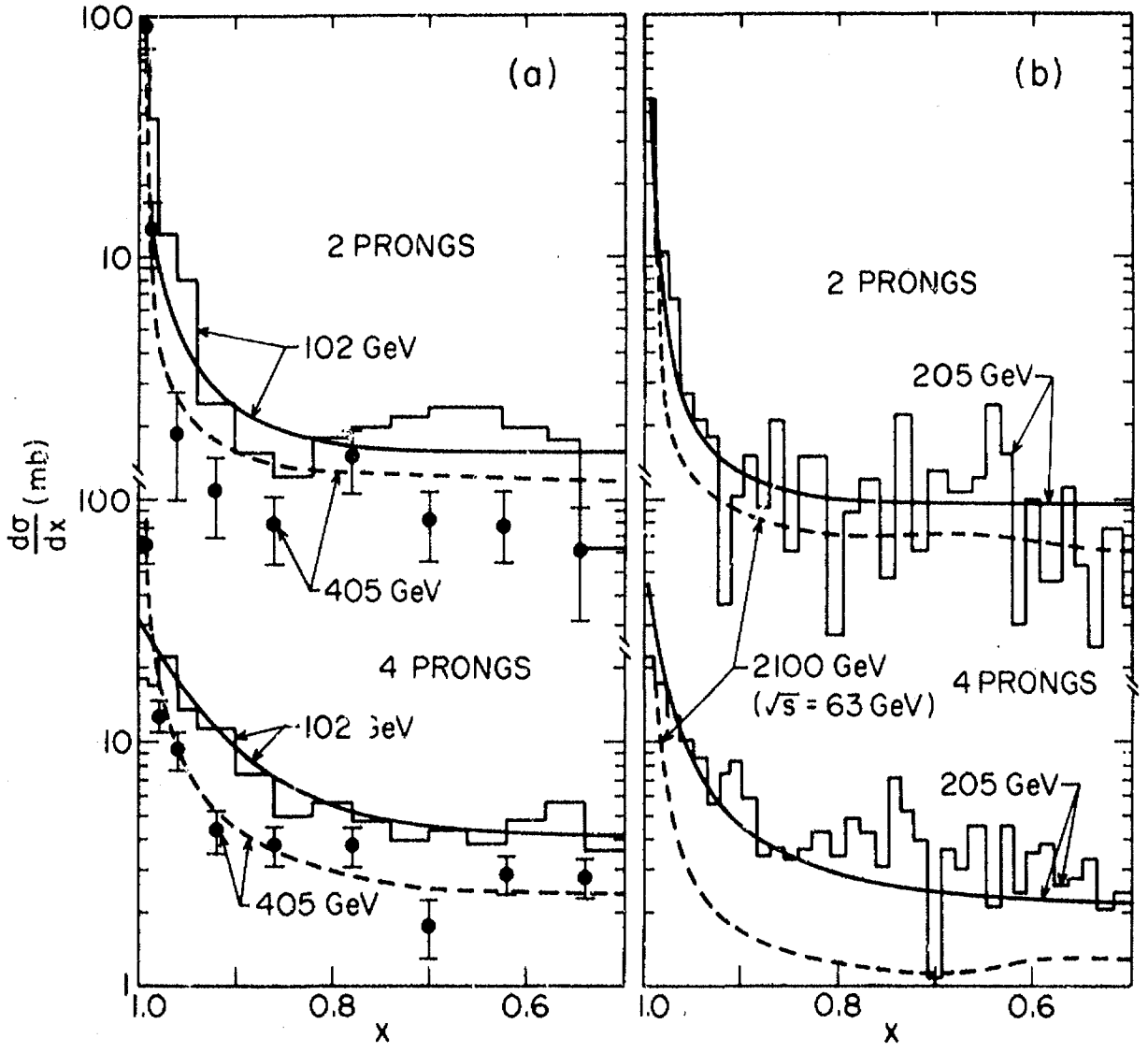
100
10
100
10
1
(a)
(b)
2 PRONGS
102 GeV
405 GeV
4 PRONGS
102 GeV
405 GeV
2 PRONGS
205 GeV
2100 GeV
(√s = 63 GeV)
4 PRONGS
205 GeV
dσ/dx (mb)
1.0
0.8
0.6
x
1.0
0.8
0.6
x

Fig. 9a,b

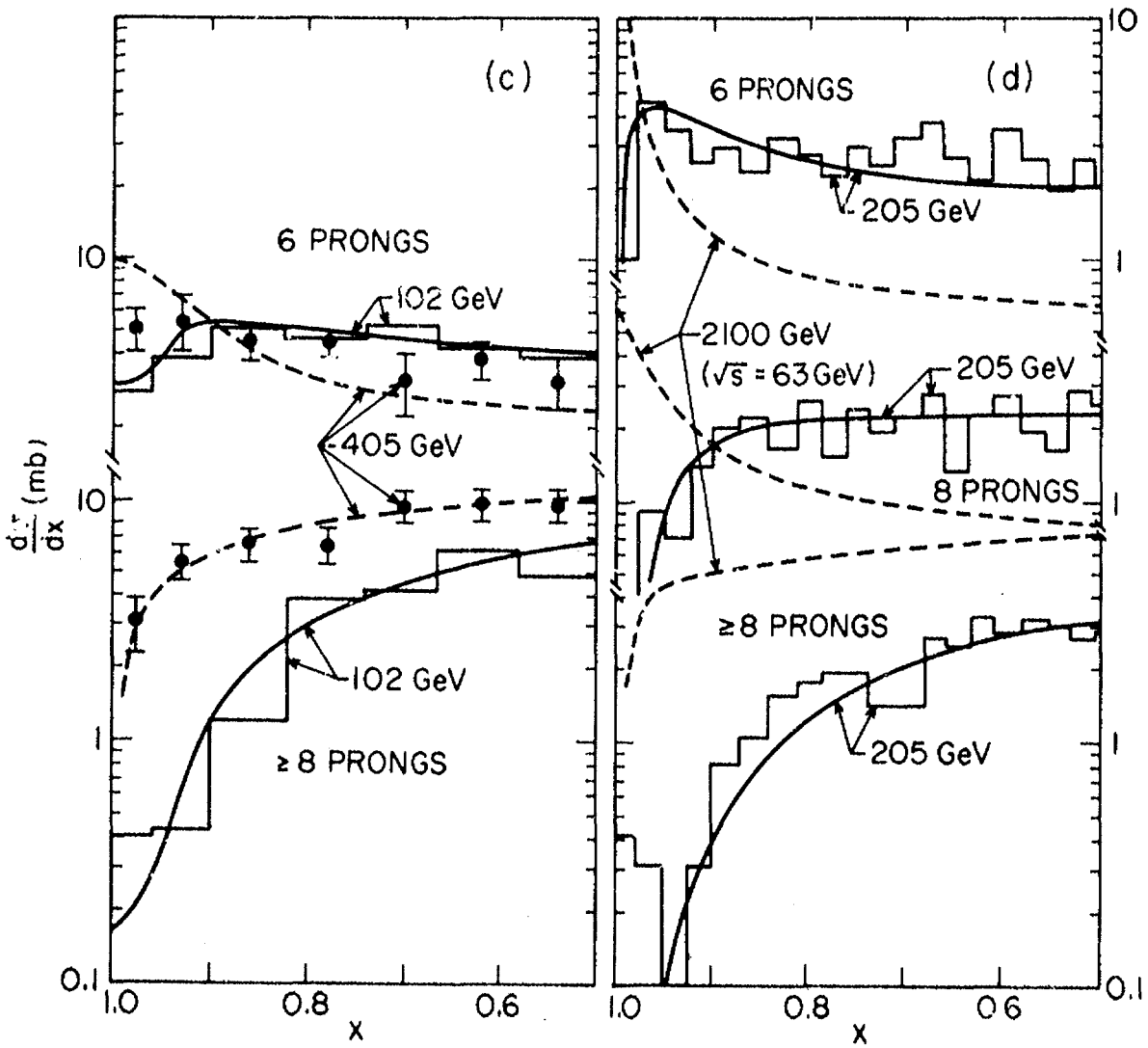
(c)
6 PRONGS
102 GeV
405 GeV
102 GeV
≥ 8 PRONGS
(d)
6 PRONGS
205 GeV
2100 GeV
(√s = 63 GeV)
205 GeV
8 PRONGS
≥8 PRONGS
205 GeV
dσ/dx (mb)
10
1
0.1
1.0
0.8
0.6
x

Fig. 9c, d

-END-

DATE FILMED

06/25/82